



## Design and Development of a Digital Controlled Dielectric Barrier Discharge (DBD) AC Power Supply for Ozone Generation

T N V Krishna<sup>1\*</sup>, P Himasree<sup>2</sup>, S Srinivasa Rao<sup>3</sup>, Yedluri Anil Kumar<sup>1</sup>, Naga Bhushanam Kundakarla<sup>4</sup> and Hee-Je Kim<sup>1\*</sup>

<sup>1</sup>Dept. of Electrical and Electronics Engineering, Pusan National University, Busandaehak-ro 63 beongil 2, Busan 46 241, Korea

<sup>2</sup>School of Electrical Engineering, Pusan National University, Busandaehak-ro 63 beongil 2, Busan 46 241, Korea

<sup>3</sup>School of Mechanical and Mechatronics Engineering, Kyungsoong University, 309 Suyeong-ro Nam-gu Busan, 48 434, Rep. of Korea

<sup>4</sup>Dept. of Chemistry, Marquette University, Milwaukee, Wisconsin 53 201, United States of America

*Received 09 July 2020; revised 15 September 2020; accepted 22 September 2020*

A digital controlled dielectric barrier discharge (DBD) AC (Alternative current) power supply is designed and investigated. The power source design with a diode bridge rectifier and PWM (Pulse Width Modulation) inverter along with driver circuits are presented. A step-up transformer is designed to carry 4.6 kW and 10 kVp-p for a dielectric barrier discharge (DBD) AC power supply and ozone generation. An STM (STMicroelectronics) microcontroller is employed to control the phase shift angle of the PWM inverter. The operating frequency of the PWM inverter is 25 kHz. Zero voltage detection can be reached and achieves maximum efficiency. Also, a high voltage transformer is included. The practical results shown that the DBD power supply can be controlled at the chosen value and extreme efficiency can be 87.45 % at 4.6 kW/10 kVp-p.

**Keywords:** Control circuit, Diode bridge rectifier, High voltage transformer, PWM inverter, STM

### Introduction

Dielectric barrier discharge (DBD) expertise schemes often require high voltage, AC (Alternative current) power systems.<sup>1-3</sup> Many of all in DBD plasma developments for environmental safety applications, like air, water, or exhaust treatment, so named DBD reactor topologies are used.<sup>4,5</sup> DBD plasma schemes as loads are very application detailed, however, they can be categorized by nonlinear voltage-power features, occasionally, for assumed working conditions and aimed chemical reactions, an optimum of supply limitations (voltage, power) can be recognized.<sup>6</sup> Modern developments contain power amplifiers (PA) with high-voltage transformers<sup>7</sup> or divergent solid-state switch based converter topologies, generally resonant ones.<sup>8</sup> Due to the resonant operation method, it is difficult to control the output power fluently; a time-averaged burst method is often used.<sup>9</sup>

A digital control power supply<sup>10,11</sup> has attracted recent attention because of the lower price, good operation with improved and assimilated power electronic peripherals, such as ADC (Analog to Digital Converters) converters<sup>12</sup> and PWM (Pulse

Width Modulation). STM (STMicroelectronics)-based microcontroller allows the execution of extra efficient control outlines, standard control hardware schemes for several stages, and flexibility. Digital controllers are less prone to aging, are eco-friendly, and have good noise reduction. The 32-bit RISC core operates at a 48 MHz frequency. Also, it has a rapid embedded memory and a wide range of improved peripherals and I/O's. The whole devices proposal typical communication interfaces one 12-bit ADC, 7 general-purpose 16-bit timers as well as a progressive control PWM timer.

Ozone (O<sub>3</sub>) is measured as an outstanding dominant oxidizer and sterilizer. Its decontamination potential is expressively greater than chlorine and other decontaminators. Currently, ozone is generally used for decontaminating and dissolving in exchange for chlorine, due to the latter by goods such as smell, bad taste, and carcinogenic causes resulting from it. Certainly, ozone creates much fewer by-products and ozone itself is converted into oxygen in limited hours. Applications of ozone expertise are many and could be established in decontamination, water, and air sanitization, drug, and so on.

Sugita<sup>13</sup> achieved complete sterilization within 60–120 sec, highlighting the value of plasma as a

\*Author for Correspondence

E-mail: heeje@pusan.ac.kr; vamsik.tirumalasetty@gmail.com

more efficient instrument than autoclaving, which takes approximately one hour. 14. Summerfelt & Hochheimer<sup>14</sup> proposed a design that can produce a high voltage yield. Moreover, the efficiency of PA (Power amplifier) is 50%. The overall power given to the load is only 1 W; hence, the potential harm of this power is insignificant. On the other hand, one problem is the current spike produced when the transistor switches OFF, which causes losses and places accumulation pressure on the transistor. Placing an extra capacitor in shunt<sup>15</sup> with the load increased the total load capacitance, thereby reducing the resonating inductor condition. This technique is not necessary because it requires two supplementary mechanisms and incurs increased power loss. Another study<sup>16</sup> did not use a resonating inductor. As an alternative, the system worked at a frequency near the resonance of the transformer and the capacitive load. Mastanaiah<sup>17</sup> proposed a plasma torch initiator using an E power amplifier. The frequency of the procedure was 13.56 MHz and the output was up to 2 kV. On the other hand, this structure is large due to the current condition of the application. In the present article, we are using a digital control system for reducing the system cost, series resonant allowing the soft switching, reduction of harmonic distortion on the terminals of DBD devices, current & voltage protection circuits are designed for system protection and the system efficiency was 87.45%. These addresses have not been highlighted in the literature.

#### Comparison with Other Control Methods

Yang & Zhijian Dan<sup>18</sup> authors designed high accuracy DC regulated power supply system based on a power amplifier and closed-loop feedback controller, and a fuzzy adaptive PID control algorithm has been used to adjust the output voltage/current. On the other hand Li *et al.*<sup>19</sup> designed a digital high-voltage power supply system based on DSP control, simulated, and tested based on Matlab/Simulink/Simpower system platform. Rao *et al.*<sup>20</sup> recorded several approaches of digital control in practical implementation, such as PID controller, Type III compensator, and sliding mode controller that are designed to promote the dynamic performance of the power supply. Pu *et al.*<sup>21</sup> gave a PID model and estimated by using MATLAB to investigate the performance of the system. The mathematical model is used to describe the control process of the beam voltage and current.

#### Recent technologies

In recent technologies, a new type of all-solid-state bipolar high-level multilevel generator is proposed<sup>22</sup> and the main energy storage capacitor of this structure is charged by a high-frequency resonant power supply after uncontrolled rectification, and the bipolar pulse output can be exploited by using each submodule. A high voltage DBD plasma reactor has been developed<sup>23</sup> using an iron plane high voltage electrode, a stainless steel ground electrode, and a glass dielectric, controlled by high voltage power supply of up to 15 kV using a high voltage step-up transformer. The study of the square current source, considering the effects of the parasitic capacitance and magnetizing inductance is reported by Rueda *et al.*<sup>24</sup>, and a numerical technique is proposed and validated for finding the working ratings and waveforms of the converter. A low-budget pulsed high voltage solid-state chopper has been developed with the modular and scaled design<sup>25</sup>, and the high voltage isolation is attained by means of the magnetic decoupling. To address the issue, a wide range frequency model of OGs is presented by Tang *et al.*<sup>26</sup>, because the current through OGs is substituted by a sinusoidal current source with variable amplitude and frequency.

Compared with additional control techniques and recent scientific trends, this system is designed with a low cost of STM microcontroller. The efficiency of the controlled system is quite high. We address the driver circuits and control circuits in this article and in the driver circuit we have used zero voltage detectors and line regulation circuits. Both circuits are used to synchronize the microcontroller with the AC input signals and the ability of the power supply to preserve its listed output voltage over the deviations in the input line voltage. This is stated as the percentage variation in the output voltage compared to the variation in the input line voltage.

The goal of this research article is the development of a digital controlled DBD AC power supply for ozone generation, consisting in a power stage, a diode bridge rectifier, inverter circuit, and control design, where the output frequency could be simply controlled by STM microcontroller.<sup>27,28</sup> A laboratory experiment was carried out to study the decontamination effectiveness of an ozone generator provided by this DBD design.

In this study, the development of a digital controlled DBD AC power source for ozone

generation is shown. An AC power supply system is designed with digital control. STM microcontroller is used in this control system. The alternative high voltage output is connected with the DBD load. This power supply system using for ozone generation applications. The system achieves 87.45 % efficiency.

**Digitally Controlled AC Power Supply**

A variable AC voltage is employed as the input voltage to the system. A diode bridge rectifier circuit was developed as the early stage of the AC power supply; it converts 220V AC to a DC (Direct Current) voltage<sup>29-36</sup> which can be varied from 0 V to 300 V by a user. An inverter topology was developed and placed, which takes the DC voltage from rectifier output and varies it to a high- frequency AC output voltage. A step-up transformer<sup>37-41</sup> was developed to achieve high voltage at the output side and the 10 kV output side of the transformer was associated with the DBD load. A zero voltage detector circuit was used to synchronize the microcontroller with the AC input signals. The STM microcontroller was used for programming the online regulation, over-voltage protection, over current protection, soft-start, and PWM.

**AC Power Source Circuit**

The simplified diagram for digital control DBD AC power supply is briefly explained below in different sub-parts.

**Diode bridge rectifier**

A high voltage single-phase diode bridge rectifier was designed with four high voltage diodes, as shown in Fig. 1. The bridge rectifier converts AC power into DC power. In this design, the DC link capacitors placed following by the bridge rectifier.

**Design of PWM inverter**

A PWM inverter is developed and placed by the after DC link capacitors as presented in Fig. 2 (a). The IXFK64N50P MOSFET was used for substituting the inverter circuit. This MOSFET was used as a switching device in the PWM full-bridge inverter.<sup>42-44</sup> The chosen MOSFET allowed a 500 V and 64 A maximum. This has a lower drain-source resistance (85 m ohms) and a fast intrinsic diode. The MOSFET switches are switched alternately with a controlled duty ratio to convert input DC voltage into high-frequency AC voltage suitable for exciting the DBD load.

The developed inverter driver circuit produces two opposite PWM signs working at 25 kHz with a 0.5 μs dead band. The driver IC (Integrated Chip) “IXDN604SIA” is a dual high rapidity gate driver that is particularly well suitable for driving MOSFETs. The input of each driver is protected effectively from latch-up, and the named circuitry removes the annoying conduction and current shoot from side to side. When the Q3 and Q6 MOSFET switches were turned ON and the Q4 and Q5 switches were turned off, a positive DC voltage was gained at the output. A negative DC voltage was gained at the output when the Q4 and Q5 switches were turned ON and the Q3 and Q6 switches were turned off. The MOSFET switches were switched consecutively with a well-ordered duty ratio to alter the input DC voltage to a high-frequency AC voltage<sup>45-50</sup> appropriate for stirring the DBD load.

The inverter is measured with phase shift signals. To function the phase-shifted PWM inverter under a zero voltage detecting circuit, the working frequency

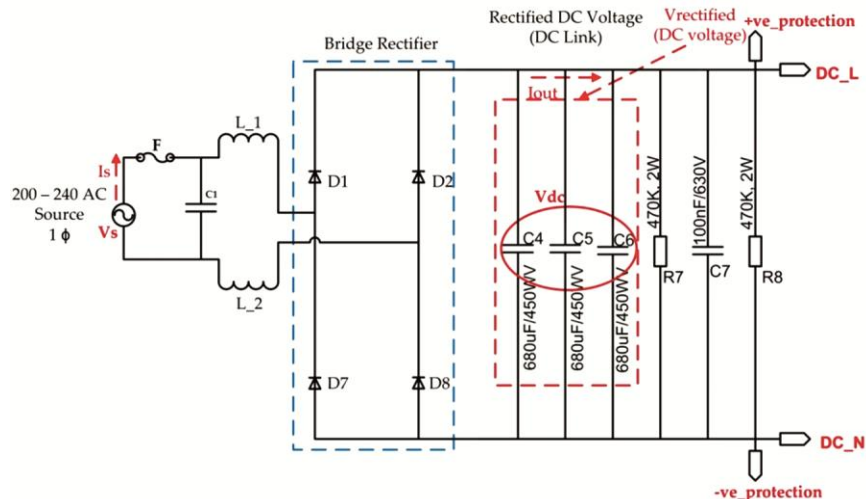


Fig. 1 — Schematic diagram of diode bridge rectifier for digital control plasma switching power supply

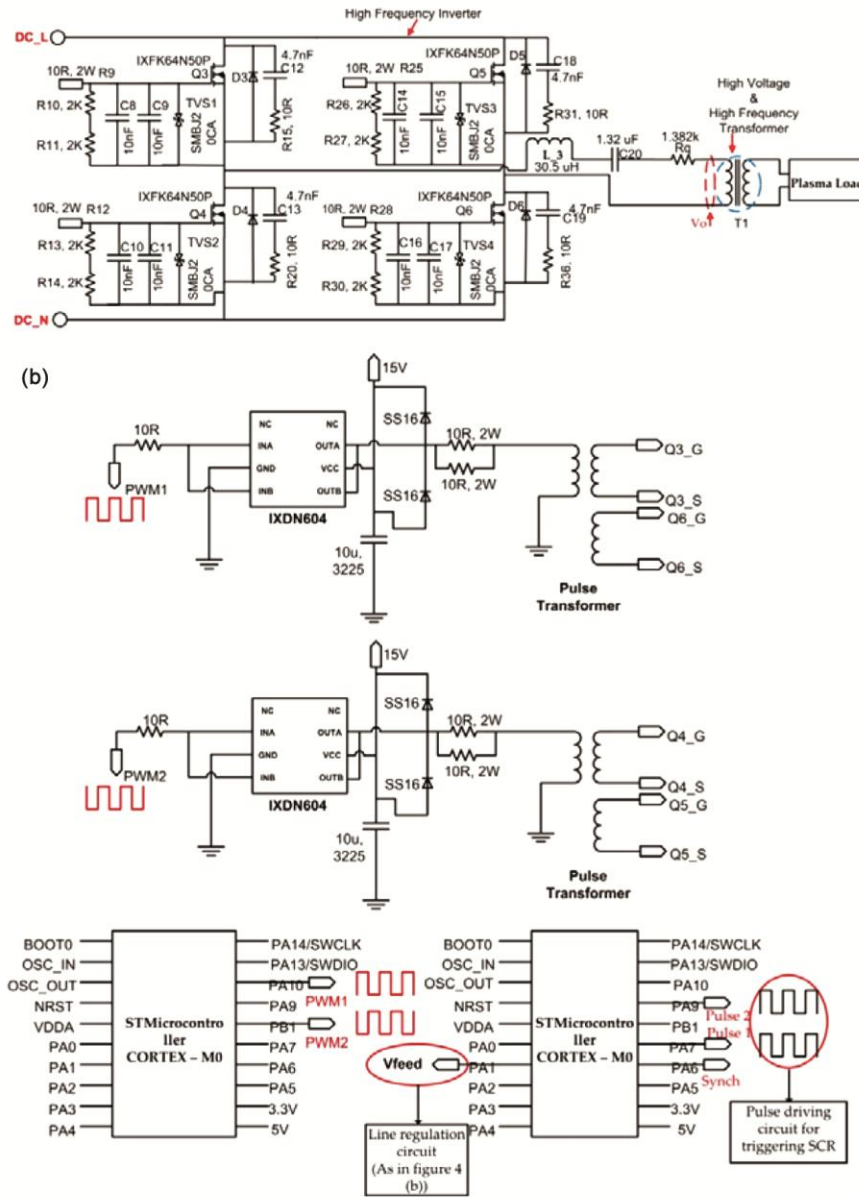


Fig. 2 — Schematic diagram of PWM inverter for digital control DBD AC power supply (a) power source; (b) Driver circuit with STM microcontroller

must be greater than the resonant tank. The resonant tank is associated with the main side of the transformer. There were four major operation modes. The power transferred to the DBD could be resolute over varying phase angles,  $\Phi_i$ , between VQ6 and VQ3, where  $\Phi_i = VQ6 < -VQ3 = VQ5 < -VQ4 <$ . The higher the phase shift angle  $\Phi_i$  is, the lesser the amplitude of the resonant voltage and output power turn out to be; and the lesser the phase shift angle  $\Phi_i$  is, the greater the amplitude of the resonant sinusoidal voltage and output power carried to the DBD turn out to be. The time break, T is from  $T_0$  to  $T_{iv}$  & is distinct

as a single period. The angle,  $\alpha_i$  is the phase angle, of which the current signal,  $i_o$  is lagging to the voltage signal,  $V_o$ . The circuit procedure equivalent to the switching designs can be investigated in four operation methods.

- Operation method I - ( $T_0 - T_i$ ): VQ3 and VQ5 are high and  $i_o < 0$  in this method. D3& Q5 are turned on. The voltage on Q3 is “0”, the value of  $i_o$  is reduced. At  $t=T_i$ ,  $i_o$  matches “0” and this method ends.
- Operation method II - ( $T_i - T_{ii}$ ): VQ3 and VQ6 are high and  $i_o > 0$  in this method. Q3 & Q6 are turned

on. The voltage on Q3 is “0” and Q3 attains a ZVC at  $T_i$ . At  $t=T_{ii}$ ,  $i_o$  extends the determined value, and this method ends.

- Operation method III - ( $T_{ii}$  -  $T_{iii}$ ): VQ4 and VQ6 are high and  $i_o > 0$  in this method. D4 & Q6 are turned on. The voltage on Q4 is “0” and the value of  $i_o$  is reduced. At  $t=T_{iii}$ ,  $i_o$  matches “0” and this method ends.
- Operation method IV - ( $T_{iii}$  -  $T_{iv}$ ): VQ4 and VQ5 are high  $i_o < 0$  in this method. Q4 & Q5 are turned on. The voltage on Q4 is “0” and Q4 attains a ZVC at  $T_{iii}$ . At  $t=T_{iv}$ ,  $i_o$  extends the determined value, and this method ends.

**High voltage transformer design**

The ferrite core transformer is designed with a C-shaped transformer core. Power ferrites are engaged as the magnetic substantial due to the more resistivity and small eddy current damages under high frequency. PL-13, U is chosen to provide the large winding turns and to achieve the insulation condition. The transformer turns are  $N_p$  &  $N_s$ , which yields  $N_p=23$ ,  $N_s=770$ .

Core cross sectional area,  $A_e = A * B = 30.3 * 18 = 545.4 \dots (1)$

Eq. (1) substitute in Eq (2) formula to determine the number of turns per volt,  $T_e$  is:

$$\frac{42}{\text{Core Area}} = \text{number of turns per volt, } T_e \dots (2)$$

Number of turns per volt,  $T_e = 0.077 \dots (3)$

Input required voltage \*  
number of turns per volt = Primary turns,  $N_p \dots (4)$

From Eq (3) and (4) substitute in below formula  
Primary turns,  $N_p = 23 \dots (5)$

Based on faradays law,

$$V = L \frac{di}{dt} = N \frac{d\phi}{dt} \dots (6)$$

$$V = N * A_e \frac{dB}{dt} \dots (7)$$

Maximum flux density,  $B_{max} = \frac{\phi}{A_e} \dots (8)$

Switching frequency is  $F_s = 25\text{kHz} \dots (9)$

From Eq (1), (8) and (9),  
 $N_p = \frac{V_s * 10^4}{4 * B_{max} * A_e * F_s} \dots (10)$

$$N_s = 33.33 * N_p \dots (11)$$

Litz wire used at the primary side of the transformer. A copper wire is used at the secondary side of the transformer and results in a minor leakage inductance. Primary winding — 0.2 mm Litz wire, 3 A/mm<sup>2</sup>; Secondary winding — AWG16 high voltage cable copper wire, 1 A/mm<sup>2</sup>.

The developed resonant frequency is around 25 kHz, and the inductor is 30.5 uH. Toprovide a high voltage to the DBD, the transformer of the turn’s ratio is 23 turns and 770 turns.

**Control Circuits for Digital Plasma**

The STM32F030F4P6 microcontroller IC was manufactured by STMicroelectronics. STM32F030F4P6 is a minimum system board (cortex-M0). The microcontroller frequency up to 48 MHz, high-speed embedded memories, anda wide range of enhanced peripherals and I/Os. All devices offer standard communication interfaces, one 12-bit ADC, seven general-purpose 16-bit timers, and an advanced-control PWM timer. The PLL is not enabled, thus the external clock drives the Cortex-M0 CPU directly.

The controller was realized with a low-cost single-chip 32-bit MCU(microcontroller unit) controller. This MCU mainly designed for cost-effective applications. STM32F030F4P6 MCUs association real-time performance and advanced architecture. As a minimal ready-to-run system, this board integrates micro USB(Universal Serial Bus) power supply interface, ISP/SWD(In-System Programming/Serial Wire Debug) programming/debugging interface, and boot mode selection and so on to take you into the ARM (Advanced RISC Machine) Cortex world easily. This IC allows synchronization of the AC input signals, regulation of the designed system, and varying the phase position of the PWM waveforms produced by the STM microcontroller.

The control circuits for the digital plasma power supply are represented in Fig. 3. The zero voltage detection circuit is shown in Fig. 3(a). Zero voltage detectors are used to synchronize the microcontroller with the AC input signals.

The line regulation circuit is presented in Fig. 3(b). The line regulation is the ability of the power supply to preserve its listed output voltage over the deviations in the input line voltage. This is stated as the percentage variation in the output voltage compared to the variation in the input line voltage.

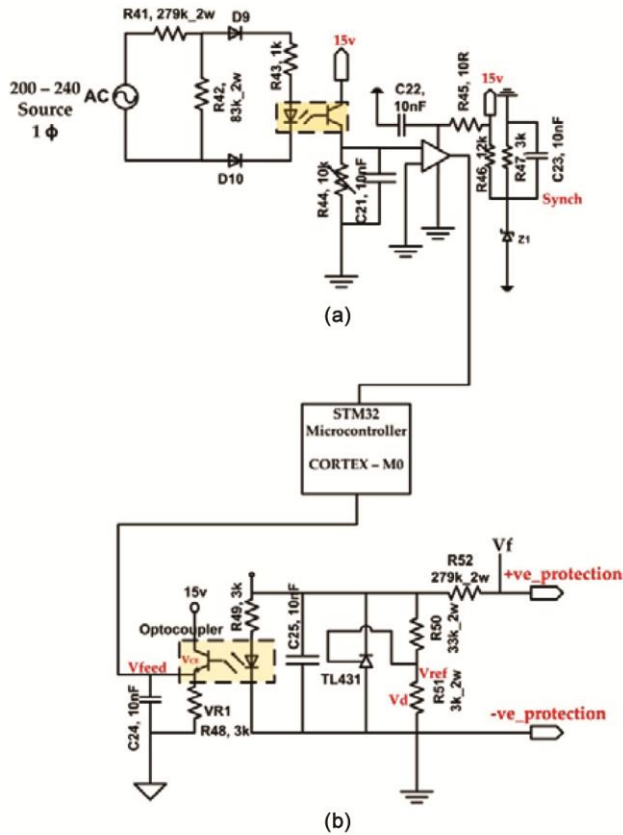


Fig. 3 — (a) Zero voltage detector circuit; (b) Line regulation circuit)

#### Setup Execution and Parameters

The proposed digital controlled DBD AC power supply was verified experimentally. The single-phase 220VAC, 60Hz power was used as an input to the circuit. The designed system is made with an inverter that is designed with “IXFK64N50P” MOSFET switches and the driver circuit is designed with the “IXDN604SIA” gate drive ICs. This inverter is connected with a transformer to increase the boosting up the output voltage.

Full-bridge phase-shifted inverter model was designed and verified with a rated power of 5000 W. The main conditions and the range of components are listed in Table 1. The rectified DC voltage was 300 V, and a MOSFET with 500 V and 64 A was selected. The considered resonant frequency was 25 kHz. To supply a high voltage to the DBD, a transformer with a high step-up ratio was used.

#### Simulation Results

The simulation results of the digital controlled DBD AC power supply by using Psim (Power sim) software are presented in Fig. 4. The single-phase

Table 1 — Specifications of digital control AC power supply

Parameter	Ratings
Input voltage	200 V AC-240 V AC
Output power	4600 W
Output voltage	10 kV <sub>p-p</sub>
Switching frequency	25 kHz
DC link voltage	300 V
MOSFET switches	IXFK64N50P
Series resonant inductor L <sub>3</sub>	30.5 uH
DC link capacitor	2040 uF
Transformer turns ratio	23:770
Transformer leakage inductance	33.33 uH

200–240 V AC is applied as an input to the diode rectifier and followed by the DC link. The DC power is applied as an input to the IGBT inverter and converts DC into AC power. The IGBT inverter provides the alternating voltage and current to the transformer. The high voltage transformer and rectifier have the task of generating voltage up to 10 kV<sub>p-p</sub>. The inverter operating frequency is 25 kHz. The input voltage ( $V_{ac}$ ), DC voltage ( $V_{dc}$ ), rectifier voltage ( $V_{rec}$ ), and waveforms of gate signals ( $V_{q3q6}$ ,  $V_{q4q5}$ ) are shown in Fig. 4(a). The primary voltage of the transformer ( $V_{prim}$ ) and the output voltage of power supply ( $V_{out}$ ) are shown in Fig. 4(b).

In this design, the simulation is carried out to prove the working operation. ZCS turn on & ZVS turn off of the IGBT’s can be reached by using the resonant circuit. The starting current of resonant topology can be partial.

#### Experimental Setup and Real-time Results

The experimental setup of the power supply for DBD is presented in Fig. 5(a). The power supply working is discussed below based on real-time results. To verify the circuits, the results are carried out with a variable AC voltage and different input power.

The output voltage ( $V_o$ ) waveform of the transformer secondary side is employed to the DBD load, as shown in Fig. 5(b), while the output current signal ( $i_o$ ) waveform of the transformer secondary side flows through the DBD load as shown in Fig. 5(c). The high-frequency PWM inverter output waveforms and gate signals are shown in Fig. 5(d). The inverter output and high-frequency square wave voltages were obtained from the DC input voltage from the bridge rectifier circuit as shown in Fig. 5(e) and it shows the two complementary 50% duty cycle PWM signals produced by the digital PWM controller. The two complementary PWM control

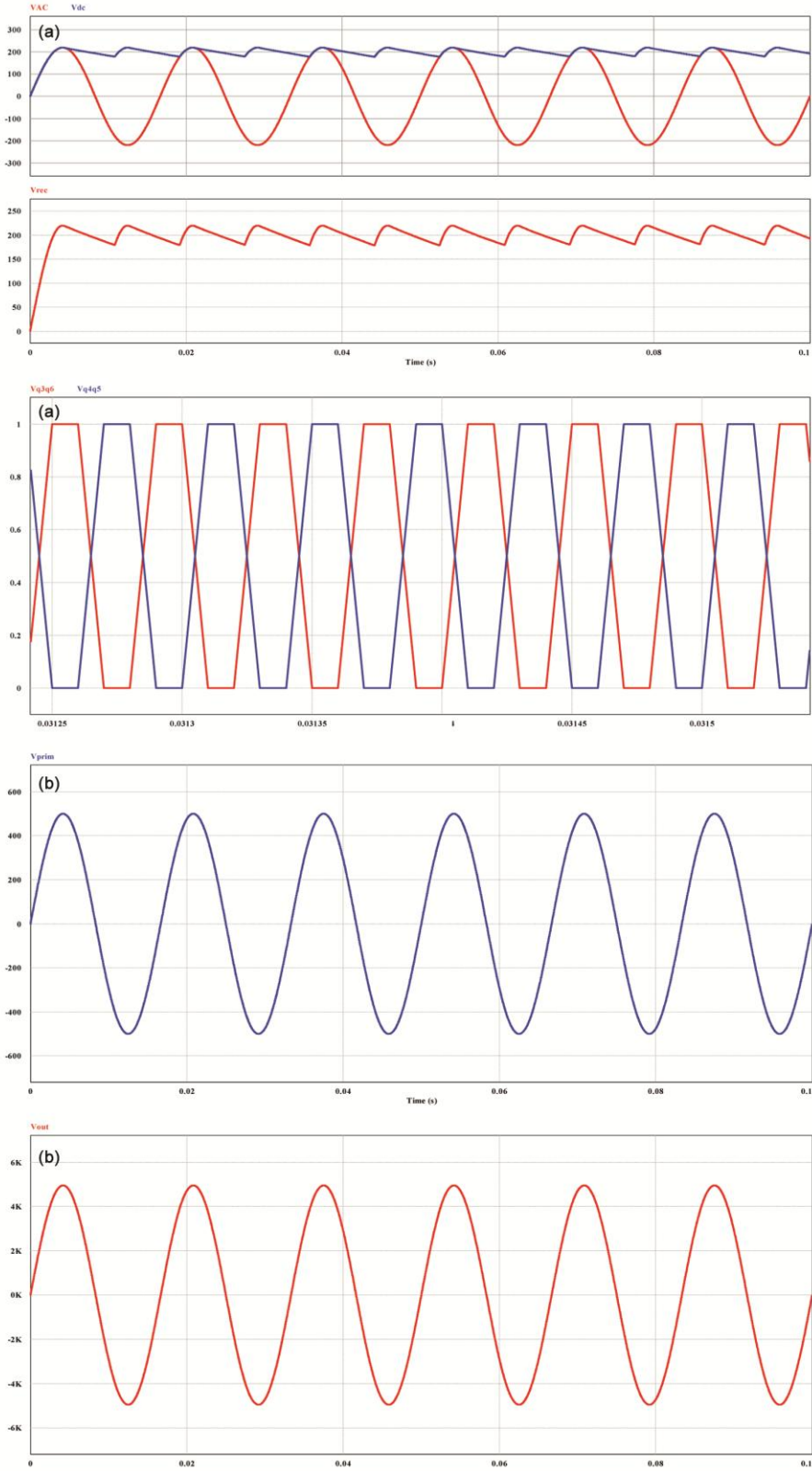


Fig. 4 — Simulation results of power supply circuit: (a) input power supply ( $V_{AC}$ ), DC voltage ( $V_{DC}$ ) and rectifier voltage ( $V_{rec}$ ); (b) Transformer primary voltage ( $V_{prim}$ ), and output voltage ( $V_{out}$ )

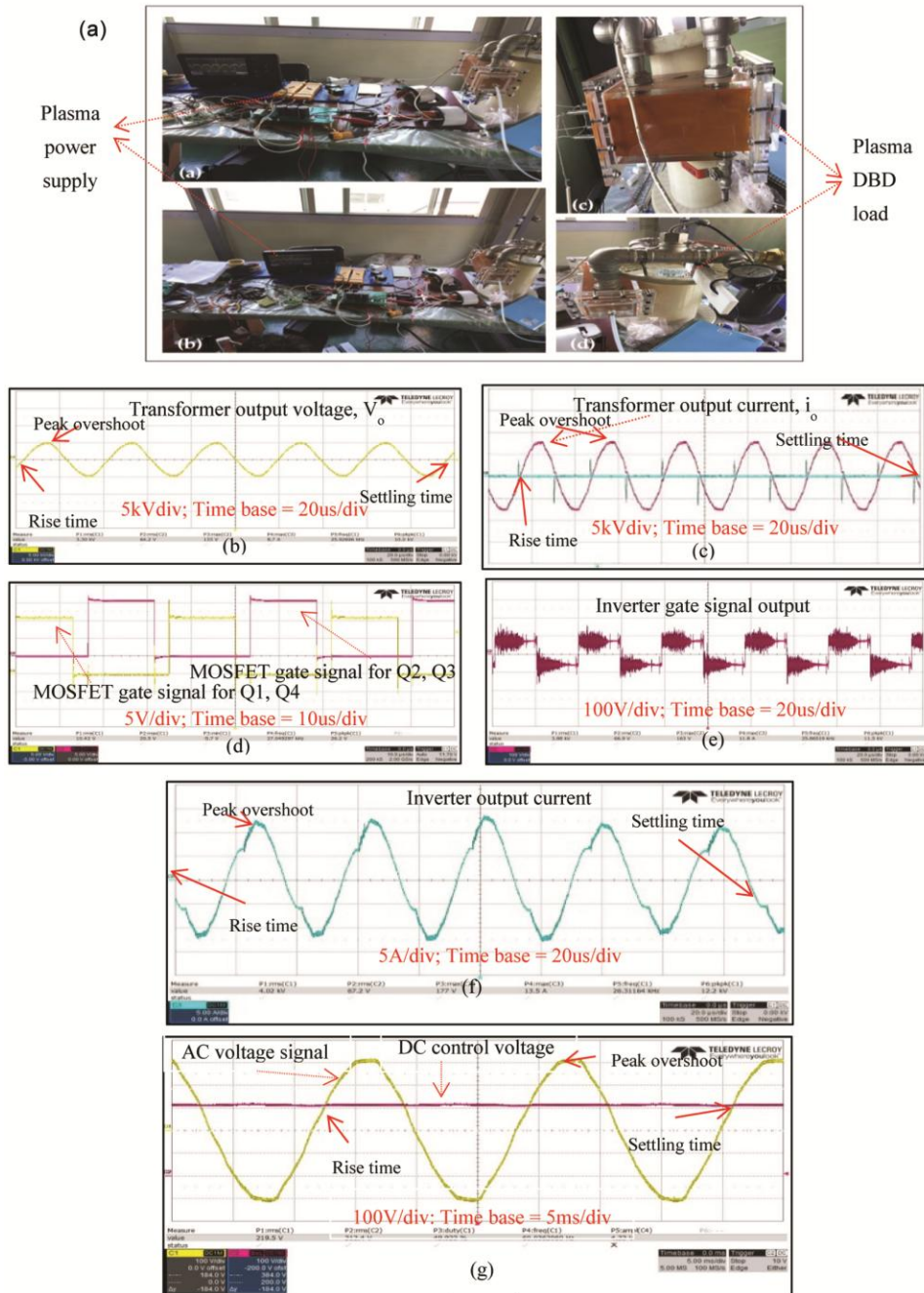


Fig. 5 — Real time results of plasma DBD power supply: (a) Experimental setup; (b) transformer output voltage,  $V_o$  (power supply output); (c) transformer output current,  $i_o$ ; (d) inverter gate signals; (e) inverter gate signal output; (f) inverter output current; (g) DC voltage from the single phase AC sinewave with different input power

signals are synchronized with each other and consist of a dead band, which avoids short circuits in full bridge. The controlled PWM signals were applied to the gate terminal of the MOSFET switches to switch the MOSFET on and off. The output current waveform of inverter (5 A/div) is shown in Fig. 5(f). The output current of the inverter side was changed to

a sinewave because of the series-connected filter. The DC voltage is converted from the single-phase AC sine wave with different input power as shown in Fig. 5(g).

**Experimental Results**

Below are the calculations for output power carried to the load and efficiency of the system.

The voltage applied to the resonant tank  $V_o$  is

$$V_o = V_{mi} \left[ \cos \left( \omega_{sw}t - \frac{\Phi}{2} \right) + \cos \left( \omega_{sw}t + \frac{\Phi}{2} \right) \right] = 2V_{mi} \cos \left( \omega_{sw}t \right) \cos \left( \frac{\Phi}{2} \right) \frac{4}{\pi} V_{dc} * \cos \left( \omega_{sw}t \right) \cos \left( \frac{\Phi}{2} \right) \dots (12)$$

The voltage RMS value is

$$V_{o,rms} = \frac{\frac{4}{\pi} V_{dc} * \cos \left( \omega_{sw}t \right) \cos \left( \frac{\Phi}{2} \right)}{\sqrt{2}} = \left( \frac{2\sqrt{2}}{\pi} \right) V_{dc} \cos \left( \frac{\Phi}{2} \right) \dots (13)$$

The standardized switching angular frequency is defined as  $\omega_{Nr} = \omega_{sw} / \omega_{ra}$ , where  $\omega_{ra}$  is the series resonant angular frequency. The switching angular frequency as  $\omega_{sw} = 2\pi * f_{sw}$ , where  $f_{sw}$  is the switching frequency.

The RMS value of the current “ $i_o$ ” employed to the resonant tank is

$$i_{o,rms} = \frac{V_{(o,rms)}}{|Z_e|} = \frac{\left( \frac{2\sqrt{2}V_{dc} \cos \left( \frac{\Phi}{2} \right) \cdot \cos \alpha_i}{\pi} \right)}{2\sqrt{2}V_{dc} \cos \left( \frac{\Phi}{2} \right)} = \frac{1}{(\pi) \cdot \sqrt{\left( 1 + P^2 \right) \cdot \left( \omega_{Nr} - \left( \frac{1}{\omega_{Nr}} \right) \right)^2}} \dots (14)$$

The load resistance  $R_q$  is,

$$R_q = \frac{V_{o,rms}}{i_{o,rms}}$$

The load resistance is,  $P_{out} = V_{o,rms} * i_{o,rms} * \cos \alpha_i = i_{o,rms}^2 * R_q$

$$= \frac{\left( \frac{2\sqrt{2} \cdot V_{dc} \cdot \cos \alpha_i \cdot \cos \left( \frac{\Phi}{2} \right)}{\pi} \right)^2 \cdot R_q}{2\sqrt{2} \cdot V_{dc}^2 \cdot \cos^2 \left( \frac{\Phi}{2} \right) \cdot R_q} = \frac{1}{(\pi^2) \cdot \left( 1 + P^2 \right) \cdot \left( \omega_{Nr} - \left( \frac{1}{\omega_{Nr}} \right) \right)^2} \dots (15)$$

Under the condition that  $R_q = 21.73K$  ohm,  $\omega_{Nr} = 1.1$ .

The output power supplied to the load  $P_{out}$  is as presented in Eq. (15). It needs to do compound multiplication in accumulation to significant the phase variance  $\alpha_i$  among the voltage & current.

The system's efficiency is,  $\eta = \left( \frac{P_{out}}{P_{in}} \right) 100$

$$= \left( \frac{2\sqrt{2} \cdot V_{dc}^2 \cos^2 \left( \frac{\Phi}{2} \right) \cdot R_q \cdot P_{in}}{(\pi^2) \cdot \left( 1 + P^2 \right) \cdot \left( \omega_{Nr} - \left( \frac{1}{\omega_{Nr}} \right) \right)^2} \right) 100$$

The inverter efficiency is,  $\eta_{inv} = \left( \frac{P_{inv} - ac}{P_{rec} - dc} \right) 100$

$$= \left( \frac{4700}{5260} \right) 100 = 89.35\%$$

To determine the output power delivered to the load  $P_{out}$  is as shown in Eq. (15). It needs to do complex multiplication in accumulation to significant the phase variance  $\alpha_i$  between the voltage and current.

The system's efficiency is,

$$\eta = \left( \frac{P_{out}}{P_{in}} \right) 100 = \left( \frac{5000}{5260} \right) 100 = 95\% \dots (16)$$

To straight determine the output power  $P_{out}$  as presented in Eq. (17), it wants to complex multiplication in addition to expressive the phase difference  $\alpha_i$  among voltage and current. In the present article, one used the fitting curve to analyze the output power with simple adding and deduction procedures only. With this technique, it can get the estimated power by simple scheming steps & can speed up the calculation procedure.

$$P_{out} = K_v \cdot V_{o,rms} + K_i \cdot i_{o,rms} - K\Phi_i \cdot \Phi_i \dots (17)$$

The electrical phase is calculated in degrees with 360 degrees consistent to the whole cycle. A sinusoidal voltage is related to the cosine or sine of the phase.

$$\text{The phase angle } A_T = A_{max} * \sin (\omega_t \pm \Phi)$$

where,  $A_{max}$  = amplitude of the signal;  $\omega_t$  = angular frequency of the signal;  $\Phi$  = phase angle in degree or radians that the signal has moved either left or right from the location point.

The ozone production with different input voltage and applied voltage flow rates are presented in Fig. 6. The result presents that the ozone production starts at a voltage of 7.0 kV<sub>p-p</sub> (210 V input voltage); from 7.0 kV<sub>p-p</sub> (210 V input voltage) the ozone production kept increasing in each voltage rate. The high ozone production is noted at 10 kV<sub>p-p</sub> (240 V input voltage) for different flow rates.

**Performance of the Developed Model with Respect to Simulation Model**

Finally, we consider the results between the developed model with respect to the simulation model by measuring the AC output power of DBD AC power supply. We measured the developed model results by using regulation and without regulation circuit. We designed a line regulation circuit with an optoisolated feedback circuit. The DC power generated by the bridge rectifier while varying AC input voltage and  $V_{feed}$  also varied in the regulation

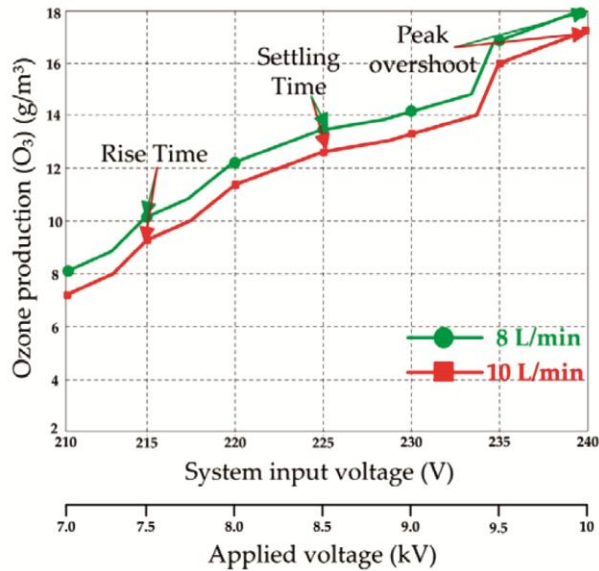


Fig. 6 — Ozone production vs different input voltage and applied voltage flow rates

Table 2 — Variation at the DC output and  $V_{\text{feed}}$  in with and without regulation circuit

Input $V_{\text{AC}}$	Without line regulation		With line regulation	
	Output $V_{\text{DC}}$	$V_{\text{feed}}$	Output $V_{\text{DC}}$	$V_{\text{feed}}$
240	310	2.64	299	2.78
230	299.5	2.64	291.3	2.74
220	290	2.64	290	2.64
210	273	2.64	285	1.99
200	258	2.64	273	0.89

circuit. The differentiation of the DC output power and  $V_{\text{feed}}$  are given in Table 2.

The developed model electrical waveforms recorded by Teledyne Lecroy (350 MHz, 2 GS/s). The voltage pulse was measured by Teledyne Lecroy high voltage probe. The current was measured by a current monitor. The simulation model was simulated by P<sub>SIM</sub> (Power SIM). The results of the developed model and theoretical values are almost matched. The developed model and simulation model of AC power generations during experimental and simulations were compared in Table 3.

#### Performance Analysis

The prototype of the digital controlled DBD AC power supply was constructed as described in previous sections. A complete picture of the power supply can be seen in Figs 1 and 2. Among the research of DBD, simulation is one of the common and useful ways. The simulation results of the DBD power supply are shown in Fig. 4. Further information

Table 3 — Comparison of developed model and simulation model AC power generations

Input AC Voltage	Developed Model (AC Power Generation)	Simulation Model (AC Power Generation)
240	4.6 kW	4.57 kW
230	4.57 kW	4.52 kW
220	4.54 kW	4.49 kW
210	4.5 kW	4.45 kW
200	4.48 kW	4.4 kW

Table 4 — Quality indices

Controller	Peak overshoot	Settling time	Rise time
STM microcontroller	52.51	7	9

Table 5 — Error indices

Controller	Error indices (Designed System)			
	ISE	IAE	ITSE	ITAE
STM microcontroller	64.50	12.15	120.25	5465

Here, ISE = Integral Square Error; IAE = Integral Absolute Error; ITSE = Integral Time Square Error; ITAE = Integral Time Absolute Error

about simulation results and parameters are also given. But, simulation technique is more complicated and time-consuming when used for long period and for different designs and models.

The line regulation circuit used to regulate the output power due to the zero voltage detector circuit. The output power decreases with an increased operating frequency and a zero voltage detector circuit is achieved for the whole power range. The peak applied voltage plays an important role in ozone generation.

When the resonant tank works at resonance, it is resistive and later the resonant frequency can be derivative. The operating frequency and tank gain at resonance with variant C20. The resonance frequency increases with decreased C20, which results in high power density. However, the tank gain of the resonant converter diminishes in the meantime.

The quality indices are presented in Table 4 for overshoot, settling time and peak overshoot and rise time for the proposed STM controller. The STM controller has quite better in case of performance. The settling time of the STM controller is 7 seconds and the rise time is 9 seconds when compared with the other controllers.<sup>51</sup>

Likewise, error indices are presented in Table 5 for the STM controller in terms of ISE, IAE, ITSE, ITAE. These indices are analyzing the good performance of the controller.

## Conclusions

This study evaluated a dielectric barrier discharge AC power supply with a digital control system for ozone generation. The presented DBD system was controlled with digital control and pulse gate driver circuit. The working frequency of the PWM inverter was 25 kHz. Zero voltage detection could be reached and the efficiency was improved. Lastly, a design with 4.6 kW and 10 kVp-p was produced in the laboratory. A step-up transformer was also added to restrict the determined voltage, and under-voltage, condition operation could be avoided. The DBD AC power supply verified experimentally and achieved maximum efficiency of 87.4% at 4.6 kW/10 kVp-p.

The novelty of this system is designed with a low cost of microcontroller which is an STM microcontroller. The efficiency of the controlled system is quite high compare with the other technologies. We address the driver circuits and control circuits in this article, these both circuits are used to synchronize the microcontroller with the AC input signals and the ability of the power supply to preserve its listed output voltage over the deviations in the input line voltage. This is stated as the percentage variation in the output voltage compared to the variation in the input line voltage.

## Future Scope

The present research work successfully verified and in the future, we are going to design a 60 kV high voltage power supply for commercial applications in the private and public sectors. We are trying to achieve more efficiency and good stability than previously designed power supplies.

## Acknowledgement

This study was supported by Brain Korea 21 Center for Creative Human Resource Development Program for IT Convergence of Pusan National University.

## References

- Kogelschatz U, (2003) Available from; 10.1023/a:1022470901385;https://dx.doi.org/10.1023/a:1022470901385.
- Gadria B & R, Roth J R, Montie T C, Kelly-Wintenberg K, Tsai P P-Y, Helfritsch D J, Feldman P, Sherman D M, Karakaya F, Chen Z, UTK Plasma Sterilization Team, Sterilization and plasma processing of room temperature surfaces with a one atmosphere uniform glow discharge plasma, *Surf Coat Technol*, **131** (2000) 528–542.
- Kim Y, Characteristics of dielectric barrier glow discharges with low-frequency generator in nitrogen, *J Korean Ph Soc*, **43(5)** (2003) 732–737.
- Kuraica M M, Obradović B M, Manojlović D, Ostojić D R & Purić J, Ozonized water generator based on coaxial dielectric-barrier-discharge in air, *Vacuum*, **73(3-4)** (2004) 705–708. Available from 10.1016/j.vacuum.2003.12.093;https://dx.doi.org/10.1016/j.vacuum.2003.12.093.
- Wagner H E, The barrier discharge: basic properties and applications to surface treatment, *Vacuum*, **71(3)** (2003) 417–436.
- Nomoto Y, Ohkubo T, Kanazawa S & Adachi T, Improvement of ozone yield by a silent-surface hybrid discharge ozonizer, *IEEE Trans Ind Appl*, **31(6)** (1995) 1458–1462, available from: 10.1109/28.475741;https://dx.doi.org/10.1109/28.475741.
- Francke K P, Rudolph R & Miessner H, (2003) Available from: 10.1023/a:1022412718224;https://dx.doi.org/10.1023/a:1022412718224.
- Casanueva R, Azcondo F J & Bracho S, Series-parallel resonant converter for an EDM power supply, *J Mater Process Technol*, **149(1-3)** (2004) 172–177, Available from: 10.1016/j.jmatprotec.2003.10.038;https://dx.doi.org/10.1016/j.jmatprotec.2003.10.038.
- Fujita H & Akagi H, Control and performance of a pulse-density-modulated series-resonant inverter for corona discharge processes, *IEEE Trans Ind Appl*, **35(3)** (1999) 621–627, Available from: 10.1109/28.767013; https://dx.doi.org/10.1109/28.767013.
- Kurimoto Y, A high precision power supply for fast pulse current with a digital control system. *IEEE Trans Appl Supercond*, **26(4)** (2016): 1–4, Available from: 10.1109/tasc.2016.2521443;https://dx.doi.org/10.1109/tasc.2016.2521443.
- Kurokawa F & Furukawa Y, High performance digital control switching power supply, in *16<sup>th</sup> International Power Electronics and Motion Control Conference and Exposition* (Turkey) (2014) 21–24.
- Sun Y, A novel high-rate hybrid window ADC design for monolithic digitally-controlled DC-DC converters, in *IEEE International Symposium on Circuits and Systems*, 2017, 28–31.
- Sugita H, Application of ozone disinfection to remove *Enterococcus seriolicida*, *Pasteurella piscicida*, and *Vibrio Anguillarum* from seawater, *Appl Environ Microbiol*, **58(12)** (1992) 4072–4075.
- Summerfelt S T & Hochheimer J N, Review of ozone processes and applications as an oxidizing agent in aquaculture (1997), Available from: 10.1577/1548-8640(1997)059<0094: roopaa>2.3.co;2;https://dx.doi.org/10.1577/1548-8640(1997)059<0094: roopaa>2.3.co;2.
- Cho M, Disinfection of water containing natural organic matter by using ozone-initiated radical reactions, *Appl Environ Microbiol*, **64(4)** (2003) 2284–2291.
- Burleson G R, Murray T M & Pollard M, Inactivation of viruses and bacteria by ozone, with and without sonication, *Appl Microbiol*, **29(3)** (1975) 340–344, Available from: 10.1128/aem.29.3.340-344.1975;https://dx.doi.org/10.1128/aem.29.3.340-344.1975.
- Mastanaiah N, A computational diagnostic tool for understanding plasma sterilization, in *49<sup>th</sup> AIAA Aerospace Sciences Meeting including the New Horizons Forum and Aerospace Exposition*, 2012, 4–7.
- Yang W, Huang J & Dai Z, Design of a high-precision DC regulated power supply system, in *IEEE 4<sup>th</sup> Information*

- Technology, Networking, Electronics and Automation Control Conference*, 1212–1216.
- 19 Li H, Tang J & Lin L, Design of digital control high-voltage DC power supply, *12<sup>th</sup> International Symposium on Computational Intelligence and Design (ISCID)* 19–22.
  - 20 Rao S, Veena K & Chakravarthi S, Design and performance analysis of digital control laws for low power high frequency switching power supply, in *IEEE 2<sup>nd</sup> International Conference on Power and Energy Applications*, 51–55.
  - 21 Pu Y, Liu G, Lin A, Wang Z, Wang J, Wu Z & Jiang W, Shengyuan Zhang & Yong Luo, PID modeling and experiment of the hot test of gyrotron traveling wave tubes. *IEEE Trans plasma sci*, **47(6)** (2019) 2812–2817.
  - 22 Jiang S, Qiu L, Li Z, Zhang L & Rao J, A new all-solid-state bipolar high-voltage multilevel generator for dielectric barrier discharge, *IEEE transactions on plasma science*, **48(4)** (2020) 1076–1081, Available from: 10.1109/tps.2020.2975216; <https://dx.doi.org/10.1109/tps.2020.2975216>.
  - 23 El-Zein A, Talaat M, El-Aragi G & El-Amawy A. The characteristics of dielectric barrier discharge plasma under the effect of parallel magnetic field, (2020), Available from: 10.1109/tps.20202977640; <https://dx.doi.org/10.1109/tps.20202977640>.
  - 24 Rueda V, Wiesner A, Diez R & Piquet H, Power Estimation of a Current Supplied DBD Considering the Transformer Parasitic Elements. *IEEE transactions on industry applications*.**55(6)** (2019): 6567–6575. Available from: 10.1109/tia.2019.2933519; <https://dx.doi.org/10.1109/tia.2019.2933519>.
  - 25 Koliadimas A, Apostolopoulos D & Svarnas P, Kiriakis Sklias, Dimitrios Athanasopoulos, Epaminondas D, Mitronikas, A Microcontroller-based modular pulsed H V power supply: desing, implementation, and tests on dbd-based plasmas, *IEEE transactions on plasma science*, **47(3)** (2019) 1621–1628.
  - 26 Tang X, Li Z & Zhang M, A Wide-range frequency model for dielectric barrier discharge type ozone generators powered by series resonant inverters. *IEEE Access*, **7** (2019) 124309–124314, Available from: 10.1109/access.2019.2901718; <https://dx.doi.org/10.1109/access.2019.2901718>.
  - 27 Mastanaiah N, Inactivation of yeast cells using dielectric barrier discharge, in *48<sup>th</sup> AIAA Aerosp Sci Meeting* (2010) 4–7.
  - 28 Alonso J M, Low-power high-voltage high-frequency power supply for ozone generation, *IEEE Trans Ind Appl* **40(2)** (2004) 414–421.
  - 29 Ponce-Silva M, Single-switch power supply based on the class E shunt amplifier for ozone generators, in *IEEE Power Electron. Specialists Conference (PESC) 2007*, 17–21.
  - 30 Pérez-Nicoli P & Silveira F, Maximum efficiency tracking in inductive power transmission using both matching networks and adjustable AC-DC converters, *IEEE Trans Microw Theory Tech*, **66(7)** (2018) 3452–3562, Available from: 10.1109/tmtt.2018.2831676; <https://dx.doi.org/10.1109/tmtt.2018.2831676>.
  - 31 Kant P & Singh B, A multi-pulse AC-DC converter fed 5-level NPC inverter based VCIMD, *IEEMA Engineer Infinite Conference (eTechNXT)* (2018).
  - 32 Gautam S & Gupta R, Balanced control of multilevel AC-DC converter with cascaded H-bridge cells, *IEEE UP Section Conference on Electrical Computer and Electronics* (2015).
  - 33 Lv Z, Distributed coordinate control based on state-of-charge for bidirectional power converters in a hybrid AC/DC Micro grid, *Energies*, **11(4)** (2018) 1–15.
  - 34 Salas-Puente R A, Power management of the DC Bus connected converters in a hybrid AC/DC microgrid tied to the main grid, *Energies*, **11(4)** (2018) 1–22.
  - 35 Yang Y, Multi-objective coordinate planning of distributed generation and AC/DC hybrid distribution networks based on a multi-scenario technique considering timing characteristics, *Energies*, **10(12)** (2017) 1–29.
  - 36 Pejmanfar R, Haghifam M, Soleymani S & Tavassoli B, Large signal stabilization of hybrid AC/DC micro-grids using nonlinear robust controller, *Energies*, **10(12)** (2017) 1985, Available from: 10.3390/en10121985; <https://dx.doi.org/10.3390/en10121985>.
  - 37 PorsA, Browne N(2008).
  - 38 Mohns E, Chunyang J, Badura H & Raether P, A fundamental step-up method for standard voltage transformers based on an active capacitive high-voltage divider, *IEEE Trans Instrum Measur*, **68(6)** (2019) 2121–2128, Available from: 10.1109/tim.2018.2880055; <https://dx.doi.org/10.1109/tim.2018.2880055>.
  - 39 Park K B, High step-up boost converter integrated with a transformer-assisted auxiliary circuit employing quasi-resonant operation, *IEEE Transactions on Power Electronics*, **27(4)** (2012) 1974–1984.
  - 40 C KS (2002)
  - 41 Furukawa K, A high step-up DC-DC converter using transformer with intrinsic voltage-doubler, in *IEEE International Symposium in Circuits and Systems* (2015) 2097–2100.
  - 42 Namboodiri A, Wani S, Bipolar U & Inverter P, *International Journal for Innovative Research in Science & Technology*, **1(7)** (2014) 237–243.
  - 43 Choi J S & Kang F S, *Seven-Level PWM Inverter Employing Series-Connected Capacitors Paralleled to a Single DC Voltage Source*, **62(6)** (2015) 3448–3459.
  - 44 Osaretin C A, Edeko F, Design and implementation of a PWM based 50 Hz 12 V DC / 220 V AC 1.5 kVA Inverter, *J electr electron eng*, **13(1)** (2016) 25–29.
  - 45 Gautam S, *AC/ DC/ AC converter based on parallel and cascaded multilevel DC / AC converter* (2012).
  - 46 Nahavandi A, Single stage DC-AC boost converter, *7<sup>th</sup> Power Electronics and Drive Systems Technologies Conference (PEDSTC)* (2016) 362–366.
  - 47 Sato K, Aging simulation of SiC-MOSFET in DC-AC converter, in *IEEE Electron Devices Technology and Manufacturing Conference (EDTM)* (2017) 119–121.
  - 48 Xiao W & Zhang B, Switching rule based on min-projection strategy for single phase DC-AC converter, *IEEE Applied Power Electronics Conference and Exposition*, 2015, 2394–2398.
  - 49 Hou C C & Su H P(2014).
  - 50 Hwu K I & Yau Y, One-comparator counter-based PWM control for DC-AC converter, in *IEEE International Symposium on Industrial Electronics*, 2009, 1813–1816.
  - 51 Karthick S, Kumar S, K& Mohan S, Relative analysis of controller effectiveness for vertical plane control of an autonomous underwater vehicle, in *OCEANS 2016-Shanghai*, 2016, 1–6.